Commun. Comput. Phys.
doi: 10.4208/cicp.OA-2016-0120

Vol. **22**, No. 1, pp. 182-201
July 2017

Efficient Numerical Solution of Dynamical Ginzburg-Landau Equations under the Lorentz Gauge

Huadong Gao*

School of Mathematics and Statistics, Huazhong University of Science and Technology, Wuhan 430074, P.R. China.

Received 26 July 2016; Accepted (in revised version) 22 November 2016

Abstract. In this paper, a new numerical scheme for the time dependent Ginzburg-Landau (GL) equations under the Lorentz gauge is proposed. We first rewrite the original GL equations into a new mixed formulation, which consists of three parabolic equations for the order parameter ψ, the magnetic field $\sigma=\mathrm{curl}\mathbf{A}$, the electric potential $\theta=\mathrm{div}\,\mathbf{A}$ and a vector ordinary differential equation for the magnetic potential $\mathbf{A}$, respectively. Then, an efficient fully linearized backward Euler finite element method (FEM) is proposed for the mixed GL system, where conventional Lagrange element method is used in spatial discretization. The new approach offers many advantages on both accuracy and efficiency over existing methods for the GL equations under the Lorentz gauge. Three physical variables ψ, σ and θ can be solved accurately and directly. More importantly, the new approach is well suitable for non-convex superconductors. We present a set of numerical examples to confirm these advantages.

AMS subject classifications: 65M12, 65M22, 65M60

Key words: Ginzburg-Landau equations, Lorentz gauge, fully linearized scheme, FEMs, magnetic field, electric potential, superconductivity.

1 Introduction

This paper is concerned with efficient numerical methods for the time-dependent Ginzburg-Landau (GL) equations

$$\begin{cases} \eta\dfrac{\partial\psi}{\partial t}+i\eta\kappa\Phi\psi+\left(\dfrac{i}{\kappa}\nabla+\mathbf{A}\right)^2\psi+(|\psi|^2-1)\psi=0, & \text{in } \Omega\times(0,T], \quad (1.1)\\ \dfrac{\partial\mathbf{A}}{\partial t}+\nabla\Phi+\mathbf{curl}\,\mathbf{curl}\,\mathbf{A}+\mathrm{Re}\left(\dfrac{i}{\kappa}\psi^*\nabla\psi\right)+|\psi|^2\mathbf{A}=\mathbf{curl}\,\mathbf{H}_e, & \text{in } \Omega\times(0,T], \quad (1.2)\end{cases}$$

*Corresponding author. *Email address:* huadong@hust.edu.cn (H. Gao)

 ©2017 Global-Science Press

https://doi.org/10.4208/cicp.OA-2016-0120 Published online by Cambridge University Press

with the following boundary and initial conditions

$$\left(\frac{i}{\kappa}\nabla\psi+\mathbf{A}\psi\right)\cdot\mathbf{n}=0,\quad \mathbf{curl}\,\mathbf{A}\times\mathbf{n}=\mathbf{H}_e\times\mathbf{n}, \qquad \text{on } \partial\Omega\times[0,T], \tag{1.3}$$

$$\psi(x,0)=\psi_0(x),\quad \mathbf{A}(x,0)=\mathbf{A}_0(x), \qquad \text{in } \Omega, \tag{1.4}$$

where Ω is a bounded domain in $\mathbb{R}^3$. In the GL equations (1.1)-(1.4), the complex scalar function ψ is the order parameter, the real vector-valued function $\mathbf{A}$ is the magnetic potential, and the real scalar function Φ is the electric potential. ψ^* denotes the complex conjugate of the function ψ. Physically, $|\psi|^2$ denotes the density of the superconducting electron pairs. $|\psi|^2=1$ and $|\psi|^2=0$ represent the perfectly superconducting state and the normal state, respectively, while $0<|\psi|^2<1$ represents a mixed (vortex) state. The real vector-valued function $\mathbf{H}_e$ is the external magnetic field, κ (positive) is the Ginzburg-Landau parameter and η (positive) is a dimensionless constant. In the rest of this paper, we set $\eta=1$ for the sake of simplicity.

We refer to [3,11] for the detailed description of the Ginzburg-Landau model in superconductivity. Theoretical analyses of the GL equations have been well done, see [3,8,20] and references therein. Numerical methods for solving the GL equations have also been investigated extensively; see [1,6,7,10,13–21,23–29]. It is well-known that the GL equations admit the gauge invariance property, see [11,12]. Two popular gauges are the temporal gauge and the Lorentz gauge. Under the temporal gauge, the GL equations are defined by

$$\begin{cases} \dfrac{\partial\psi}{\partial t}+\left(\dfrac{i}{\kappa}\nabla+\mathbf{A}\right)^2\psi+(|\psi|^2-1)\psi=0, & \text{in } \Omega\times(0,T], \quad (1.5)\\ \dfrac{\partial\mathbf{A}}{\partial t}+\mathbf{curl}\,\mathbf{curl}\,\mathbf{A}+\mathrm{Re}\left(\dfrac{i}{\kappa}\psi^*\nabla\psi\right)+|\psi|^2\mathbf{A}=\mathbf{curl}\,\mathbf{H}_e, & \text{in } \Omega\times(0,T]. \quad (1.6) \end{cases}$$

As fewer terms are involved, the GL equations under the temporal gauge looks simpler. We refer to [10,16,18,24,25,27,28] for the numerical methods for the GL equations under the temporal gauge. However, it should be noted that Eq. (1.6) for $\mathbf{A}$ is a degenerate parabolic equation, where $\|\mathbf{curl}\,\mathbf{A}\|_{L^2}$ is not equivalent to $|\mathbf{A}|_{H^1}$. Due to this degeneracy, in [10,23] an extra perturbation term $-\epsilon\nabla\mathrm{div}\,\mathbf{A}$ was added to Eq. (1.6) for $\mathbf{A}$. Therefore, the results obtained in [10,24] depend on the parameter ϵ. By taking $\Phi=-\mathrm{div}\,\mathbf{A}$, the GL equations under the Lorentz gauge can be written as

$$\begin{cases} \dfrac{\partial\psi}{\partial t}-i\kappa(\mathrm{div}\,\mathbf{A})\psi+\left(\dfrac{i}{\kappa}\nabla+\mathbf{A}\right)^2\psi+(|\psi|^2-1)\psi=0, & \text{in } \Omega\times(0,T], \quad (1.7)\\ \dfrac{\partial\mathbf{A}}{\partial t}-\nabla\mathrm{div}\,\mathbf{A}+\mathbf{curl}\,\mathbf{curl}\,\mathbf{A}+\mathrm{Re}\left(\dfrac{i}{\kappa}\psi^*\nabla\psi\right)+|\psi|^2\mathbf{A}=\mathbf{curl}\,\mathbf{H}_e, & \text{in } \Omega\times(0,T], \quad (1.8) \end{cases}$$

https://doi.org/10.4208/cicp.OA-2016-0120 Published online by Cambridge University Press

with the following boundary and initial conditions

$$\frac{i}{\kappa}\nabla\psi\cdot\mathbf{n}=0,\quad \mathbf{curl}\,\mathbf{A}\times\mathbf{n}=\mathbf{H}_e\times\mathbf{n},\quad \mathbf{A}\cdot\mathbf{n}=0, \qquad \text{on } \partial\Omega\times[0,T], \tag{1.9}$$

$$\psi(x,0)=\psi_0(x),\quad \mathbf{A}(x,0)=\mathbf{A}_0(x), \qquad \text{in } \Omega. \tag{1.10}$$

It should be noted that under the Lorentz gauge Eq. (1.8) for $\mathbf{A}$ is parabolic. Because of the uniform parabolic property of $\mathbf{A}$, analysis of the equation is easier and computation becomes more stable. Several numerical methods with rigorous error analyses had been proposed for the GL equations under the Lorentz gauge, see [6,7,14,15,20,21]. Among these works, for the two-dimensional GL equations Chen and Hoffmann in [7] provided a sub-optimal L^2 estimate for a weakly nonlinear scheme with conventional finite element approximations. In [24], Mu and Huang presented an optimal L^2 estimate for an alternating Crank-Nicolson FEM with mesh ratio condition $\tau=h^{\frac{11}{12}}$ for the two-dimensional model and $\tau=h^2$ for the three-dimensional model. An optimal error estimates without any mesh ratio restrictions for a linearized Crank-Nicolson FEM was provided in [14] by the authors.

Besides $|\psi|$, the magnetic field $\sigma=\mathrm{curl}\mathbf{A}$ and the electric potential $\theta=\mathrm{div}\mathbf{A}$ are also desirable. However, conventional methods only solve for ψ_h and $\mathbf{A}_h$ and then use certain numerical differentiation to calculate curl$\mathbf{A}$ and div$\mathbf{A}$. Obviously, this approach will reduce the accuracy of the solution. Also, it has been shown that numerical differentiation will introduce "corner singularity" near the domain corners, see numerical experiments for a unit square domain in [15,23]. Another crucial issue is that analyses in [6,7,14,24] require a strong regularity of the exact solutions, which further implies that the domains must be smooth or convex. However, the spatial regularity of the GL equations under the Lorentz gauge on a non-convex polygon may be lower that H^1 (see [20]). In [9], Chrysafinos and Hou proved that, in order to ensure the convergence of conventional FEMs for parabolic equations, the minimum spatial regularity of the exact solution is $H^{1+s}(\Omega)$ for a certain $s>0$. Therefore, in case of the domain is a non-convex polygon conventional Lagrange FEMs for the GL equations under Lorentz gauge may converge to a spurious solutions. We refer to the numerical experiments reported in [1,15,21] for the spurious convergence phenomena of conventional FEMs. Superconducting devices usually involve complicated geometries which include non-convex domains, see [1,19,25]. Thus, it is important to design numerical methods that can solve the GL equations correctly with complex geometries. We shall mention that several mixed methods had been suggested for solving the GL equations. By introducing curl$\mathbf{A}$ and div$\mathbf{A}$ as two new variables, Chen in [6] proposed and analyzed a mixed finite element method for the two-dimensional GL equations under Lorentz gauge. More recently, for both two- and three-dimensional GL equations under Lorentz gauge, the authors [15] suggested a linearized Galerkin-mixed FEM where only one extra variable curl$\mathbf{A}$ was introduced. Numerical examples were given to indicate that the scheme in [15] converge to the true solution on non-convex domains. However, the linear system generated in the mixed method is not symmetric positive definite and requires special iterative solvers, see discussions in [2,5]. To solve

https://doi.org/10.4208/cicp.OA-2016-0120 Published online by Cambridge University Press

the GL equations correctly by conventional Lagrange FEM, the authors [16] presented a new mixed formulation for the GL equations under the temporal gauge and proposed a fully linearized FEM. The method in [16] can solve for ψ, $\sigma = \mathrm{curl}\mathbf{A}$ and $\mathbf{A}$ directly. However, numerical differentiation is needed to compute $\mathrm{div}\mathbf{A}$. We shall also mention that Li and Zhang proposed a methods based on the Hodge decomposition in [21] for the two-dimensional GL equations under the Lorentz gauge. Conventional Lagrange FEM is used in spatial discretization. The algorithm in [21] needs to solve six linear systems at each time step and extra numerical efforts are needed to compute $\mathbf{A}$, $\mathrm{curl}\mathbf{A}$ and $\mathrm{div}\mathbf{A}$.

Motivated by the above, the main purpose of the present paper is to extent the method in [16] to the GL equations under the Lorentz gauge. The key step is to rewrite the original GL equations into a new system by taking curl and div to the equation for $\mathbf{A}$. Then, we get a new mixed GL equations which consists of four equations of four variables: ψ, $\sigma = \mathrm{curl}\mathbf{A}$, $\theta = \mathrm{div}\mathbf{A}$ and $\mathbf{A}$. A fully linearized Lagrange FEM is introduced for the new mixed GL equations. Only four linear systems need to be solved at each time step. We remark that the proposed method can solve $\mathrm{div}\mathbf{A}$ efficiently. We also compare the proposed method with conventional FEMs. Numerical experiments show that the proposed method needs less computational costs and provides more accurate numerical solutions for $\mathrm{curl}\mathbf{A}$ and $\mathrm{div}\mathbf{A}$. Furthermore, we use the proposed method to investigate the vortex motion in an L-shape superconductor. The numerical solutions converge to the true vortex pattern and the method is well suitable for modeling superconductors with complex geometries.

This paper is organized as follows. In Section 2, we derive a new mixed formulation of the Ginzburg-Landau equations (MGL) under the Lorentz gauge, and propose a fully linearized scheme with finite element approximations for solving the MGL equations. In Section 3, we test the convergence rate and stability of the proposed method and compare it with a conventional FEM. In Section 4, we use the proposed method to compute the vortex patterns for the square and L-shape superconductors.

2 A mixed formulation and a linearized finite element method

In this section, we present a new mixed formulation and a numerical method for the GL equations under Lorentz gauge. For simplicity, we restrict to the GL equations in two-dimensional space. The following standard calculus operators in two-dimensional space will be used

$$\mathrm{div}\mathbf{A} = \frac{\partial A_1}{\partial x} + \frac{\partial A_2}{\partial y}, \qquad \nabla\psi = \left(\frac{\partial \psi}{\partial x}, \frac{\partial \psi}{\partial y}\right)^T,$$
$$\mathrm{curl}\mathbf{A} = \frac{\partial A_2}{\partial x} - \frac{\partial A_1}{\partial y}, \qquad \mathbf{curl}\,\psi = \left(\frac{\partial \psi}{\partial y}, -\frac{\partial \psi}{\partial x}\right)^T.$$

With the above notations, the two-dimensional GL equations under the Lorentz gauge

https://doi.org/10.4208/cicp.OA-2016-0120 Published online by Cambridge University Press

is defined by

$$\begin{cases} \dfrac{\partial\psi}{\partial t}-i\kappa(\mathrm{div}\,\mathbf{A})\psi+\left(\dfrac{i}{\kappa}\nabla+\mathbf{A}\right)^2\psi+(|\psi|^2-1)\psi=0, & \text{in } \Omega\times(0,T], \quad (2.1)\\ \dfrac{\partial\mathbf{A}}{\partial t}-\nabla\mathrm{div}\,\mathbf{A}+\mathbf{curl}\,\mathrm{curl}\,\mathbf{A}+\mathrm{Re}\left(\dfrac{i}{\kappa}\psi^*\nabla\psi\right)+|\psi|^2\mathbf{A}=\mathbf{curl}\,H_e, & \text{in } \Omega\times(0,T], \quad (2.2)\end{cases}$$

with the following boundary and initial conditions

$$\frac{i}{\kappa}\nabla\psi\cdot\mathbf{n}=0,\quad \mathrm{curl}\mathbf{A}=H_e,\quad \mathbf{A}\cdot\mathbf{n}=0, \qquad \text{on } \partial\Omega\times[0,T], \quad (2.3)$$

$$\psi(x,0)=\psi_0(x),\quad \mathbf{A}(x,0)=\mathbf{A}_0(x), \qquad \text{in } \Omega. \quad (2.4)$$

We take the curl on both sides of Eq. (2.2). With the notation $\sigma=\mathrm{curl}\mathbf{A}$, we obtain a new equation for σ as follows

$$\frac{\partial\sigma}{\partial t}-\Delta\sigma+\mathrm{Re}\left(\frac{i}{\kappa}\mathbf{curl}\psi\cdot\nabla\psi^*\right)+|\psi|^2\sigma-\mathbf{A}\cdot\mathbf{curl}|\psi|^2=-\Delta H_e, \quad (2.5)$$

with the following boundary and initial conditions

$$\sigma=H_e, \qquad \text{on } \partial\Omega\times[0,T], \quad (2.6)$$

$$\sigma(x,0)=\mathrm{curl}\mathbf{A}_0(x), \qquad \text{in } \Omega. \quad (2.7)$$

Similarly, we take the div on both sides of Eq. (2.2). With the notation $\theta=\mathrm{div}\mathbf{A}$, we can derive a new equation for θ below

$$\frac{\partial\theta}{\partial t}-\Delta\theta+\mathrm{Re}\left(\frac{i}{\kappa}\psi^*\Delta\psi\right)+|\psi|^2\theta+\mathbf{A}\cdot\nabla|\psi|^2=0, \quad (2.8)$$

with the following boundary and initial conditions

$$\frac{\partial\theta}{\partial\mathbf{n}}=0, \qquad \text{on } \partial\Omega\times[0,T], \quad (2.9)$$

$$\theta(x,0)=\mathrm{div}\mathbf{A}_0(x), \qquad \text{in } \Omega. \quad (2.10)$$

Then, a new mixed formulation of the Ginzburg-Landau equations (MGL) is defined by

$$\begin{cases} \dfrac{\partial\psi}{\partial t}-i\kappa\theta\psi+\left(\dfrac{i}{\kappa}\nabla+\mathbf{A}\right)^2\psi+(|\psi|^2-1)\psi=0, & (2.11)\\ \dfrac{\partial\sigma}{\partial t}-\Delta\sigma+\mathrm{Re}\left(\dfrac{i}{\kappa}\mathbf{curl}\psi\cdot\nabla\psi^*\right)+|\psi|^2\sigma-\mathbf{A}\cdot\mathbf{curl}|\psi|^2=-\Delta H_e, & (2.12)\\ \dfrac{\partial\theta}{\partial t}-\Delta\theta+\mathrm{Re}\left(\dfrac{i}{\kappa}\psi^*\Delta\psi\right)+|\psi|^2\theta+\mathbf{A}\cdot\nabla|\psi|^2=0, & (2.13)\\ \dfrac{\partial\mathbf{A}}{\partial t}-\nabla\theta+\mathbf{curl}\sigma+\mathrm{Re}\left(\dfrac{i}{\kappa}\psi^*\nabla\psi\right)+|\psi|^2\mathbf{A}=\mathbf{curl}\,H_e, & (2.14)\end{cases}$$

https://doi.org/10.4208/cicp.OA-2016-0120 Published online by Cambridge University Press

for $x\in\Omega$, $t\in(0,T]$ with the following boundary and initial conditions

$$\left(\frac{i}{\kappa}\nabla\psi+\mathbf{A}\psi\right)\cdot\mathbf{n}=0,\quad \sigma=H_e,\quad \frac{\partial\theta}{\partial\mathbf{n}}=0,\quad \text{on } \partial\Omega\times[0,T], \tag{2.15}$$

$$\psi(x,0)=\psi_0(x),\ \sigma(x,0)=\text{curl}\mathbf{A}_0(x),\ \theta(x,0)=\text{div}\mathbf{A}_0(x),\ \mathbf{A}(x,0)=\mathbf{A}_0(x),\quad \text{in } \Omega. \tag{2.16}$$

The above MGL system consists of four equations for four unknowns ψ, σ, θ and $\mathbf{A}$, respectively. It is easy to see that the first three equations are uniformly parabolic. Therefore, ψ, $\sigma=\text{curl}\mathbf{A}$ and $\theta=\text{div}\mathbf{A}$ usually admit better regularity than $\mathbf{A}$. It should be noted that Eq. (2.13) appeared in [20] (between Eqn. (4.1) and Eqn. (4.2) of [20]), where Li and Zhang obtained the regularity of ψ, $\mathbf{A}$, curl$\mathbf{A}$ and div$\mathbf{A}$ for the two-dimensional Ginzburg-Landau equations in nonconvex polygons (see Theorem 2.1 and 2.2 of [20]). Moreover, the fourth equation (2.14) in the MGL system is an ordinary differential equation for $\mathbf{A}$, which can be solved with less computational cost. We shall present a fully linearized Galerkin FEM for solving the MGL equations (2.11)-(2.16).

We briefly introduce some notations for the standard Sobolev spaces. Let $W^{k,p}(\Omega)$ be the conventional Sobolev space defined on Ω with $H^k(\Omega):=W^{k,2}(\Omega)$. We denote by $\mathcal{H}^k(\Omega)=\{u+iv|u,v\in H^k(\Omega)\}$ the space of the complex-valued functions and by $\mathbf{H}^k(\Omega)=[H^k(\Omega)]^2$ the space of the vector-valued functions with two components. We define

$$\mathring{H}^k(\Omega)=\left\{u\,\middle|\,u\in H^k(\Omega),\quad u\big|_{\partial\Omega}=0\right\}.$$

With the above notations, the variational formulation of the MGL system (2.11)-(2.16) is to find $\psi\in L^2(0,T;\mathcal{H}^1(\Omega)\cap\mathcal{L}^\infty(\Omega))$ with $\frac{\partial\psi}{\partial t}\in L^2(0,T;\mathcal{H}^{-1}(\Omega))$, $\sigma\in L^2(0,T;H^1(\Omega))$ with $\frac{\partial\sigma}{\partial t}\in L^2(0,T;H^{-1}(\Omega))$, $\theta\in L^2(0,T;H^1(\Omega))$ with $\frac{\partial\theta}{\partial t}\in L^2(0,T;H^{-1}(\Omega))$, and $\mathbf{A}\in L^2(0,T;\mathbf{H}^0)$ with $\frac{\partial\mathbf{A}}{\partial t}\in L^2(0,T;\mathbf{H}^0)$, such that

$$\begin{cases}
(\frac{\partial\psi}{\partial t},\omega)-i\kappa\theta(\psi,\omega)+((\frac{i}{\kappa}\nabla+\mathbf{A})\psi,(\frac{i}{\kappa}\nabla+\mathbf{A})\omega) & \\
\qquad+((|\psi|^2-1)\psi,\omega)=0, & \forall\omega\in\mathcal{H}^1(\Omega), \quad (2.17)\\
(\frac{\partial\sigma}{\partial t},\xi)+(\nabla\sigma,\nabla\xi)+\left(\text{Re}\left(\frac{i}{\kappa}\mathbf{curl}\psi\cdot\nabla\psi^*\right),\xi\right) & \\
\qquad+(|\psi|^2\sigma,\xi)-(\mathbf{A}\cdot\mathbf{curl}|\psi|^2,\xi)=-(\Delta H_e,\xi), & \forall\xi\in\mathring{H}^1(\Omega), \quad (2.18)\\
(\frac{\partial\theta}{\partial t},\chi)+(\nabla\theta,\nabla\chi)-\left(\text{Re}\left(\frac{i}{\kappa}\psi^*\nabla\psi\right),\nabla\chi\right) & \\
\qquad+(|\psi|^2\theta,\chi)+(\mathbf{A}\cdot\nabla|\psi|^2,\chi)=0, & \forall\chi\in H^1(\Omega), \quad (2.19)\\
(\frac{\partial\mathbf{A}}{\partial t},\mathbf{v})-(\nabla\theta,\mathbf{v})+(\mathbf{curl}\sigma,\mathbf{v})-\left(\text{Re}\left(\frac{i}{\kappa}\psi^*\nabla\psi\right),\mathbf{v}\right) & \\
\qquad+(|\psi|^2\mathbf{A},\mathbf{v})=(\mathbf{curl}H_e,\mathbf{v}), & \forall\mathbf{v}\in\mathbf{H}^0(\Omega), \quad (2.20)
\end{cases}$$

https://doi.org/10.4208/cicp.OA-2016-0120 Published online by Cambridge University Press

for a.e. $t\in(0,T]$ with $\psi(x,0)=\psi_0(x)$, $\sigma(x,0)=\mathrm{curl}\mathbf{A}_0(x)$, $\theta(x,0)=\mathrm{div}\mathbf{A}_0(x)$ and $\mathbf{A}(x,0)=\mathbf{A}_0(x)$.

Here we simply assume that Ω is a two-dimensional polygon. The extension to more general domains is straightforward. Let $\mathcal{T}_h$ be a regular partition of Ω with $\Omega=\cup_K\Omega_K$ and mesh size $h=\max_{\Omega_K\in\mathcal{T}_h}\{\mathrm{diam}\Omega_K\}$. For a given partition $\mathcal{T}_h$, we denote by $\mathcal{V}_h^r$, V_h^r and $\mathbf{V}_h^r$ the r-th order Lagrange finite element subspaces of $\mathcal{H}^1(\Omega)$, $H^1(\Omega)$ and $\mathbf{H}^1(\Omega)$, respectively. Also we denote $\mathring{V}_h^r=V_h^r\cap\mathring{H}^1$, i.e., the Lagrange finite element subspace with zero trace. We define by Π_h the commonly used Lagrange nodal interpolation operator [4].

Let $\{t_n\}_{n=0}^N$ be a uniform partition in the temporal direction with the step size $\tau=\frac{T}{N}$, and let $u^n=u(\cdot,n\tau)$. For a sequence of functions $\{U^n\}_{n=0}^N$ defined on Ω, we denote

$$D_\tau U^n=\frac{U^n-U^{n-1}}{\tau},\quad \text{for } n=1,2,\cdots,N.$$

We are now ready to introduce our numerical method. The linearized backward Euler FEM for the MGL system (2.11)-(2.16) is to find $\psi_h^n\in\mathcal{V}_h^r$, $\sigma_h^n\in V_h^r$, $\theta_h^n\in V_h^r$ and $\mathbf{A}_h^n\in\mathbf{V}_h^r$, with $\sigma_h^n|_{\partial\Omega}=\Pi_h H_e^n$, such that for $n=1,2,\cdots,N$

$$\begin{cases}
(D_\tau\psi_h^n,\omega_h)+\dfrac{1}{\kappa^2}(\nabla\psi_h^n,\nabla\omega_h)=i(\kappa-\dfrac{1}{\kappa})(\theta_h^{n-1}\psi_h^{n-1},\omega_h)\\
\quad-\dfrac{2i}{\kappa}(\mathbf{A}_h^{n-1}\nabla\psi_h^{n-1},\omega_h)-((|\mathbf{A}_h^{n-1}|^2+|\psi_h^{n-1}|^2-1)\psi_h^{n-1},\omega_h),\quad \forall\omega_h\in\mathcal{V}_h^r, & (2.21)\\
(D_\tau\sigma_h^n,\xi_h)+(\nabla\sigma_h^n,\nabla\xi_h)=-\left(\mathrm{Re}\left(\dfrac{i}{\kappa}\mathbf{curl}\psi_h^{n-1}\cdot\nabla(\psi_h^{n-1})^*\right),\xi_h\right)\\
\quad-(|\psi_h^{n-1}|^2\sigma_h^{n-1},\xi_h)+(\mathbf{A}_h^{n-1}\cdot\mathbf{curl}|\psi_h^{n-1}|^2,\xi_h)-(\Delta H_e^n,\xi_h),\quad \forall\xi_h\in\mathring{V}_h^r, & (2.22)\\
(D_\tau\theta_h^n,\chi_h)+(\nabla\theta_h^n,\nabla\chi_h)=\left(\mathrm{Re}\left(\dfrac{i}{\kappa}(\psi_h^{n-1})^*\nabla\psi_h^{n-1}\right),\nabla\chi_h\right)\\
\quad-(|\psi_h^{n-1}|^2\theta_h^{n-1},\chi_h)-(\mathbf{A}_h^{n-1}\cdot\nabla|\psi_h^{n-1}|^2,\chi_h),\quad \forall\chi_h\in V_h^r, & (2.23)\\
(D_\tau\mathbf{A}_h^n,\mathbf{v}_h)=(\nabla\theta_h^{n-1},\mathbf{v}_h)-(\mathbf{curl}\sigma_h^{n-1},\mathbf{v}_h)-\left(\mathrm{Re}\left(\dfrac{i}{\kappa}(\psi_h^{n-1})^*\nabla\psi_h^{n-1}\right),\mathbf{v}_h\right)\\
\quad-(|\psi_h^{n-1}|^2\mathbf{A}_h^{n-1},\mathbf{v}_h)+(\mathbf{curl}H_e^n,\mathbf{v}_h),\quad \forall\mathbf{v}_h\in\mathbf{V}_h^r, & (2.24)
\end{cases}$$

where $r\geq 1$ and $\psi_h^0=\Pi_h\psi_0$, $\sigma_h^0=\Pi_h\mathrm{curl}\mathbf{A}_0$, $\theta_h^0=\Pi_h\mathrm{div}\mathbf{A}_0$ and $\mathbf{A}_h^0=\Pi_h\mathbf{A}_0$ are used at the initial time step.

Clearly, each of the first three systems can be viewed as a finite element approximation to a typical parabolic equation and the fourth one is the forward Euler scheme for a vector

https://doi.org/10.4208/cicp.OA-2016-0120 Published online by Cambridge University Press

differential equation. The corresponding linear systems can be written by

$$\begin{cases} (\mathbf{M}_\psi + \frac{\tau}{\kappa^2}\mathbf{K}_\psi)\,\psi_h^n = \mathbf{b}_\psi^{n-1}, & (2.25)\\ (\mathbf{M}_\sigma + \tau\mathbf{K}_\sigma)\,\sigma_h^n = \mathbf{b}_\sigma^{n-1}, & (2.26)\\ (\mathbf{M}_\theta + \tau\mathbf{K}_\theta)\,\theta_h^n = \mathbf{b}_\theta^{n-1}, & (2.27)\\ \mathbf{M}_A\,\mathbf{A}_h^n = \mathbf{b}_A^{n-1}, & (2.28) \end{cases}$$

where $\mathbf{M}_l$ and $\mathbf{K}_l$, $l=\psi,\sigma,\theta,A$, denote the mass matrix and stiffness matrix, respectively.

Now we have the following algorithm.

Algorithm 1.

• Step 1. For a given partition $\mathcal{T}_h$, generate the matrices $\mathbf{M}_\psi$, $\mathbf{K}_\psi$, $\mathbf{M}_\sigma$, $\mathbf{K}_\sigma$, $\mathbf{M}_\theta$, $\mathbf{K}_\theta$ and $\mathbf{M}_A$ and calculate the initial solution $\psi_h^0=\Pi_h\psi^0$, $\sigma_h^0=\Pi_h\mathrm{curl}\mathbf{A}_0$, $\theta_h^0=\Pi_h\mathrm{div}\mathbf{A}_0$ and $\mathbf{A}_h^0=\Pi_h\mathbf{A}_0$. Set $n=1$.

• Step 2. Calculate $\mathbf{b}_l^{n-1}$, $l=\psi,\sigma,\theta,A$.

• Step 3. Solve the linear systems (2.25)-(2.28) simultaneously to get ψ_h^n, σ_h^n, θ_h^n and $\mathbf{A}_h^n$.

• Step 4. If $T=n\tau$, stop. Otherwise, set $n:=n+1$ and go to Step 2.

The existence and uniqueness of the FEM solution follow directly from the fact that the coefficient matrices in (2.21)-(2.24) are symmetric and positive definite. Also it is easy to see that the proposed numerical approach is fully linearized and all terms, except three diffusion terms, are treated explicitly by the Euler scheme. At each time step, one only needs to solve four linear systems with coefficient matrices being independent of the time evolution, which can be pre-assembled at Step 1. Also our numerical results show that such a full linearization is unconditionally stable and no mesh ratio restriction condition is needed. Moreover, $\mathbf{M}_A$ is mass matrix whose condition number is independent of the mesh size h, see Table 5. For the scheme (2.21)-(2.24), under certain conditions on the domain Ω, τ and h it is possible to derive

$$\max_{0\le n\le N}\left(\|\psi_h^n\|_{L^2}^2+\|\sigma_h^n\|_{L^2}^2+\|\theta_h^n\|_{L^2}^2+\|\mathbf{A}_h^n\|_{L^2}^2\right)+\tau\sum_{m=1}^{N}\left(\|\nabla\psi_h^m\|_{L^2}^2+\|\nabla\sigma_h^m\|_{L^2}^2+\|\nabla\theta_h^m\|_{L^2}^2\right)\le C, \tag{2.29}$$

where C is a constant only depending upon the physical variables. However, for nonconvex polygons, due to linearization of the nonlinear terms and the low regularity of the exact solutions the analysis of the scheme is rather challenging.

3 Numerical results: artificial examples

In this section, we provide several numerical examples to test the convergence rate and stability of the proposed method (2.21)-(2.24). We also compare the new approach with

https://doi.org/10.4208/cicp.OA-2016-0120 Published online by Cambridge University Press

a conventional FEM for the GL equations under Lorentz gauge. All computations in this paper were done by the free software FEniCS [22] on a Linux laptop with a four core Intel 2.5GHz Processor and 7.9GB Memory.

Example 3.1. Here we consider an artificial example defined by

$$\begin{cases} \dfrac{\partial\psi}{\partial t}-i\kappa(\mathrm{div}\,\mathbf{A})\psi+\left(\dfrac{i}{\kappa}\nabla+\mathbf{A}\right)^2\psi+(|\psi|^2-1)\psi=g, & \text{in } \Omega\times(0,T], \quad (3.1)\\ \dfrac{\partial\mathbf{A}}{\partial t}-\nabla\mathrm{div}\,\mathbf{A}+\mathbf{curl}\,\mathrm{curl}\,\mathbf{A}+\mathrm{Re}\left(\dfrac{i}{\kappa}\psi^*\nabla\psi\right)+|\psi|^2\mathbf{A}=\mathbf{curl}\,H_e+\mathbf{f}, & \text{in } \Omega\times(0,T], \quad (3.2)\end{cases}$$

with the boundary and initial conditions

$$\frac{i}{\kappa}\nabla\psi\cdot\mathbf{n}=0,\quad \mathrm{curl}\,\mathbf{A}=H_e,\quad \mathbf{A}\cdot\mathbf{n}=0, \qquad \text{on } \partial\Omega\times[0,T], \quad (3.3)$$

$$\psi(x,0)=\psi_0(x),\quad \mathbf{A}(x,0)=\mathbf{A}_0(x), \qquad \text{in } \Omega, \quad (3.4)$$

where we take the unit square domain $\Omega=(0,1)^2$ and set $\kappa=1$. The functions g, $\mathbf{f}$, ψ_0 and $\mathbf{A}_0$ are chosen correspondingly to the exact solution

$$\psi=\exp(t)(\cos(\pi x)+i\cos(\pi y)),\quad \mathbf{A}=\begin{bmatrix}\exp(t+y)\sin(\pi x)\\ \exp(t+x)\sin(\pi y)\end{bmatrix} \quad (3.5)$$

with

$$H_e=\exp(t+x)\sin(\pi y)+\exp(t+y)\sin(\pi x).$$

We set the terminal time $T=0.5$ in this example.

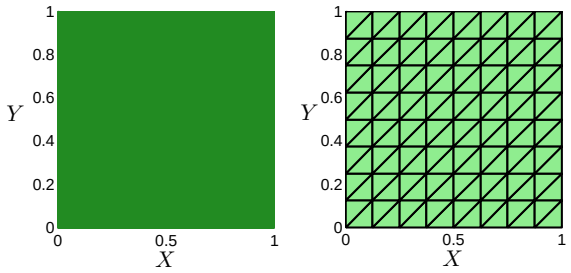


Figure 1: A uniform triangular mesh on the unit square domain with $M=8$.

In the computation, we use a uniform triangular mesh with $M+1$ vertices in each direction, where $h=\frac{\sqrt{2}}{M}$ (see Fig. 1 for the illustration with $M=8$). We solve the system (3.1)-(3.2) by the proposed method (2.21)-(2.24) with $r=1$, 2, 3. As the expected optimal convergence rate is $\mathcal{O}(\tau+h^{r+1})$ in L^2-norm, we set $\tau=\left(\frac{1}{M}\right)^{r+1}$. The L^2-norm errors of ψ_h, σ_h, θ_h, $\mathbf{A}_h$, and $\mathbf{curl}\sigma_h$ are presented in Table 1, where Err_u denotes the error

https://doi.org/10.4208/cicp.OA-2016-0120 Published online by Cambridge University Press

Table 1: L^2-norm errors of the new method for the MGL equations (Example 3.1).

$\tau=\frac{1}{M^2}(r=1)$	Err_ψ	Err_σ	Err_θ	$\mathrm{Err}_{\mathbf{A}}$	$\mathrm{Err}_{\mathbf{curl}\sigma}$
$M=32$	3.5761e-03	2.4437e-03	6.2567e-03	3.5270e-02	4.9934e-02
$M=64$	8.7709e-04	6.0871e-04	1.5389e-03	1.1904e-02	1.7099e-02
$M=128$	2.1713e-04	1.5195e-04	3.8188e-04	4.0872e-03	5.9448e-03
order	2.02	2.00	2.02	1.55	1.54
$\tau=\frac{1}{M^3}(r=2)$	Err_ψ	Err_σ	Err_θ	$\mathrm{Err}_{\mathbf{A}}$	$\mathrm{Err}_{\mathbf{curl}\sigma}$
$M=8$	3.6854e-03	5.7671e-03	4.0502e-03	5.3880e-02	6.3690e-02
$M=16$	4.6313e-04	7.4935e-04	5.1349e-04	1.2556e-02	1.5000e-02
$M=32$	5.8149e-05	9.4937e-05	6.4629e-05	3.0733e-03	3.6824e-03
order	2.99	2.96	2.98	2.07	2.06
$\tau=\frac{1}{M^4}(r=3)$	Err_ψ	Err_σ	Err_θ	$\mathrm{Err}_{\mathbf{A}}$	$\mathrm{Err}_{\mathbf{curl}\sigma}$
$M=4$	7.2859e-03	1.2374e-02	4.6362e-03	4.6541e-02	5.8295e-02
$M=8$	4.6437e-04	8.0130e-04	2.8844e-04	3.0626e-03	3.9903e-03
$M=16$	2.9080e-05	5.0248e-05	1.7959e-05	2.2175e-04	2.9583e-04
order	3.98	3.97	4.01	3.86	3.81

$\|u_h^N-u(\cdot,0.5)\|_{L^2}$. From Table 1, we can see that the convergence rate for ψ_h, σ_h and θ_h are optimal with order $\mathcal{O}(h^{r+1})$ and the convergence rate for $\mathbf{A}_h$ is one order lower. The sub-optimal convergence rate for $\mathbf{A}_h$ need further investigation. We note that the numerical solutions ψ_h, σ_h, θ_h and $\mathbf{curl}\sigma_h$ are of more interests in physics.

To test the stability of the proposed method, we solve the system (3.1)-(3.2) by the new method (2.21)-(2.24) with a quadratic finite element approximation on gradually refined meshes with $M=8$, 16, 32, 64, 128 and 256, where three fixed time steps $\tau=0.05$, 0.01, 0.001 are used. The L^2 errors of ψ_h, σ_h, θ_h and $\mathbf{A}_h$ are shown in Fig. 2. One can see from Fig. 2 that, for each fixed τ, when the mesh is refined gradually, each L^2-error function

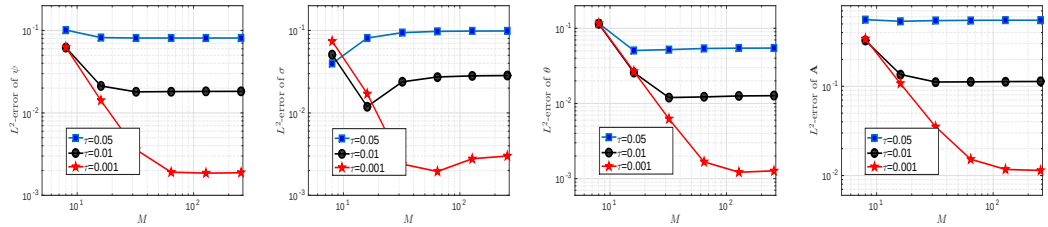


Figure 2: L^2 errors of the new approach with a quadratic element method for the MGL equations on gradually refined meshes (Example 3.1).

https://doi.org/10.4208/cicp.OA-2016-0120 Published online by Cambridge University Press

converges to a small constant of order $\mathcal{O}(\tau)$. This shows that the proposed method is unconditionally stable, i.e., the method does not require the mesh ratio condition $\tau \leq Ch^{\alpha}$ for a certain $\alpha > 0$, although the explicit Euler scheme is used for solving $\mathbf{A}$. Therefore, the proposed method is robust and large time steps can be used for practical computation in a long time period.

Example 3.2. In this example, we compare the approach (2.21)-(2.24) with a conventional FEM. A fully linearized Galerkin FEM for the above GL system (3.1)-(3.5) is to find $\psi_h^n \in \mathcal{V}_h^r$ and $\mathbf{A}_h^n \in \overline{\mathbf{V}}_h^r$, such that for $n = 1,2,\cdots,N$

$$\begin{cases} (D_\tau \psi_h^n, \omega_h) + \frac{1}{\kappa^2}(\nabla \psi_h^n, \nabla \omega_h) = i\kappa((\operatorname{div} \mathbf{A}_h^{n-1})\psi_h^{n-1}, \omega_h) - \frac{i}{\kappa}(\nabla \psi_h^{n-1}, \mathbf{A}_h^{n-1}\omega_h) \\ \qquad + \frac{i}{\kappa}(\mathbf{A}_h^{n-1}\psi_h^{n-1}, \nabla \omega_h) - ((|\mathbf{A}_h^{n-1}|^2 + |\psi_h^{n-1}|^2 - 1)\psi_h^{n-1}, \omega_h), \quad \forall \omega_h \in \mathcal{V}_h^r, \\ (D_\tau \mathbf{A}_h^n, \mathbf{v}_h) + (\operatorname{div} \mathbf{A}_h^n, \operatorname{div} \mathbf{v}_h) + (\operatorname{curl} \mathbf{A}_h^n, \operatorname{curl} \mathbf{v}_h) = -\left(\operatorname{Re}\left(\frac{i}{\kappa}(\psi_h^{n-1})^* \nabla \psi_h^{n-1}\right), \mathbf{v}_h\right) \\ \qquad - (|\psi_h^{n-1}|^2 \mathbf{A}_h^{n-1}, \mathbf{v}_h) + (H_e^n, \operatorname{curl} \mathbf{v}_h), \quad \forall \mathbf{v}_h \in \overline{\mathbf{V}}_h^r, \end{cases} \tag{3.6}$$

where $\overline{\mathbf{V}}_h^r = \{\mathbf{u} | \mathbf{u} \in \mathbf{V}_h^r, \mathbf{u} \cdot \mathbf{n} = 0|_{\partial\Omega}\}$, and the initial conditions $\psi_h^0 = \Pi_h \psi_0$ and $\mathbf{A}_h^0 = \Pi_h \mathbf{A}_0$.

We solve (3.1)-(3.5) by the conventional FEM (3.6) with the same settings in the last Example 3.1. We present the L^2-norm errors of the conventional FEM at $T = 0.5$ in Table 3. The convergence rates for ψ_h and $\mathbf{A}_h$ are optimal with the same order $\mathcal{O}(h^{r+1})$. As

Table 2: L^2-norm errors of conventional FEM (3.6) for the GL equations under Lorentz gauge (Example 3.2).

$\tau = \frac{1}{M^2}(r=1)$	Err_ψ	Err_σ	Err_θ	$\mathrm{Err}_{\mathbf{A}}$	$\mathrm{Err}_{\mathbf{curl}\sigma}$
$M=32$	6.8026e-03	1.0363e-01	2.4060e-01	6.3814e-03	
$M=64$	1.6987e-03	5.1641e-02	1.2010e-01	1.5970e-03	
$M=128$	4.2456e-04	2.5786e-02	6.0016e-02	3.9936e-04	
order	2.00	1.00	1.00	2.00	
$\tau = \frac{1}{M^3}(r=2)$	Err_ψ	Err_σ	Err_θ	$\mathrm{Err}_{\mathbf{A}}$	$\mathrm{Err}_{\mathbf{curl}\sigma}$
$M=8$	5.8137e-03	2.0044e-02	5.6738e-02	2.1110e-03	1.5965e+00
$M=16$	7.1836e-04	4.9243e-03	1.4405e-02	2.5878e-04	7.9373e-01
$M=32$	8.9307e-05	1.2266e-03	3.6284e-03	3.2015e-05	3.9577e-01
order	3.01	2.01	1.98	3.02	1.01
$\tau = \frac{1}{M^4}\ (r=3)$	Err_ψ	Err_σ	Err_θ	$\mathrm{Err}_{\mathbf{A}}$	$\mathrm{Err}_{\mathbf{curl}\sigma}$
$M=4$	1.1203e-02	1.0316e-02	1.6085e-02	3.3661e-03	2.9040e-01
$M=8$	6.9704e-04	8.9511e-04	1.7126e-03	2.1000e-04	7.2561e-02
$M=16$	4.3537e-05	9.4819e-05	2.0326e-04	1.3111e-05	1.8163e-02
order	4.00	3.38	3.15	4.00	2.00

https://doi.org/10.4208/cicp.OA-2016-0120 Published online by Cambridge University Press

numerical differentiation is used, the convergence rates for σ_h and θ_h are one-order lower and the convergence rate for curlσ_h is two-order lower. From Tables 1 and 3, It is easy to see that the new method (2.21)-(2.24) can solve for $\sigma = \text{curl}\mathbf{A}$, $\theta = \text{div}\mathbf{A}$ and $\mathbf{curl}\sigma$ more accurately than the conventional FEM (3.6).

Next, we compare the iteration numbers required by the CG solver in Examples 3.1 and 3.2. Linear element methods are used for the comparison. We use the CG algorithm without preconditioning to solve the linear systems. We set the same relative tolerance $\frac{\|\boldsymbol{r}\|_{l^2}}{\|\boldsymbol{b}\|_{l^2}} \leq 1.0\times 10^{-9}$ for these two methods. At each time step, the initial guess for the solver is provided by the numerical solution at the former time step. The average iteration numbers required are shown in Table 3. "Iter(u)" denotes the average iteration number required of variable u. From Table 3, we can see that Iter($\mathbf{A}$) is independent of the mesh size h. By noting that $\mathbf{A}$ is a vector function, it is clear that the proposed method (2.21)-(2.24) needs less computational costs and can solve the GL equations under Lorentz gauge more accurately.

Table 3: The average iteration numbers required by the new approach and the conventional FEM (Section 3).

	New approach				Conventional FEM	
$\tau = 0.01$	Iter(ψ)	Iter(σ)	Iter(θ)	Iter($\mathbf{A}$)	Iter(ψ)	Iter($\mathbf{A}$)
M=32	72.62	49.26	22.00	20.86	79.98	121.30
M=64	137.86	94.52	41.00	19.54	157.72	229.10
M=128	267.02	178.44	77.00	18.24	315.30	445.22
M=256	525.72	333.60	146.00	17.00	635.36	878.86
$\tau = 0.005$	Iter(ψ)	Iter(σ)	Iter(θ)	Iter($\mathbf{A}$)	Iter(ψ)	Iter($\mathbf{A}$)
M=32	52.00	34.02	18.00	19.89	54.04	91.27
M=64	96.40	65.37	32.00	18.55	107.43	165.79
M=128	187.70	124.21	61.00	17.36	215.30	319.44
M=256	369.90	240.40	116.85	16.00	434.94	625.59
$\tau = 0.001$	Iter(ψ)	Iter(σ)	Iter(θ)	Iter($\mathbf{A}$)	Iter(ψ)	Iter($\mathbf{A}$)
M=32	25.00	13.17	9.00	17.63	25.48	46.15
M=64	42.00	25.00	16.00	16.46	43.25	79.94
M=128	79.00	48.67	30.00	15.00	82.61	146.72
M=256	152.00	87.87	57.00	14.01	166.76	279.62

4 Simulations on vortex motion

In this section, we provide three examples on the vortex motion simulations in superconductors with different geometries. We first test the proposed method for a unit square

https://doi.org/10.4208/cicp.OA-2016-0120 Published online by Cambridge University Press

superconductor and compare the results with conventional FEM, see Example 4.1. Then, in Example 4.2 we investigate the vortex motion in an L-shape superconductor and show that the proposed method is well suitable for non-convex problems. Finally, in Example 4.3, we study the vortex motion in a circular disk with boundary defect by the new scheme.

Example 4.1. In the first example, we set the domain $\Omega=(0,1)^2$, the Ginzburg-Landau parameter $\kappa=10$ and the external applied magnetic field $H_e=3.5$. This problem have been tested by conventional FEMs [14, 23, 28], a Galerkin-mixed method [15], and a method based the two-dimensional Hodge decomposition [21]. We show the plots of the numerical solutions of $|\psi_h|$, σ_h and θ_h at $T=20$ in Fig. 3, where a linear element method on a uniform mesh with $M=128$ and $\tau=0.01$ are used. We have observed that the vortex pattern is almost stable at $T=20$. From Fig. 3, one can see that amplitude of the electric potential $\theta=\mathrm{div}\,\mathbf{A}$ is relatively small (less than 10^{-4}).

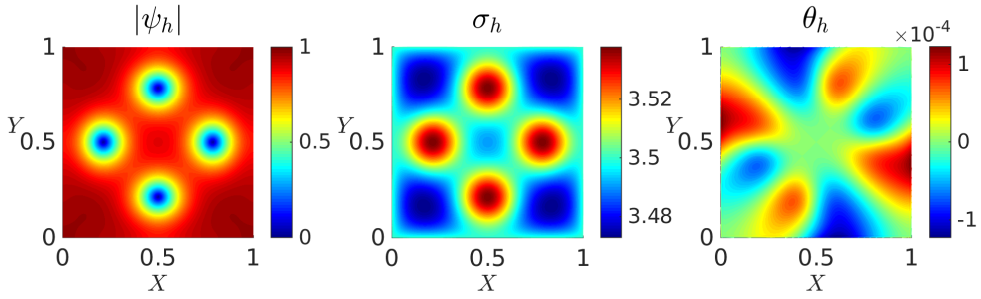


Figure 3: The numerical results at $T=20$. A linear element method on a uniform mesh with $M=128$ and time step $\tau=0.01$ are used. (Example 4.1).

To compare the computational costs of the proposed method (2.21)-(2.24) and the conventional FEM (3.6), we present the average iteration numbers of each variables in Table 4. Three different time steps $\tau=0.01$, 0.005, 0.001 and gradually refined meshes with $M=32$, 64, 128, 256 are used. Again, we set the relative tolerance $\frac{\|\boldsymbol{r}\|_{l^2}}{\|\boldsymbol{b}\|_{l^2}}\leq 1.0\times 10^{-9}$ for the CG solver (without preconditioning). From Table 4, we can see that the two methods have similar Iter(ψ). However, Iter($\mathbf{A}$) in the conventional FEM is very large. As $\mathbf{A}$ is a vector function, the total cost for the conventional FEM is larger than that of the new approach.

Furthermore, we provide the l^2-norm condition numbers of the coefficient matrices for each variable in Table 5. It is easy to see that the condition number of coefficient matrices of σ_h and θ_h are both of $\mathcal{O}(\frac{1}{h^2})$. However, the average iteration numbers required for σ_h and θ_h are quite different and Iter(θ) is much larger than Iter(σ). To make clear this phenomenon, we plot σ_h and θ_h at $T=10$, 12, 14, 16, 18 and 20 in Fig. 4. We also show the evolution of $\frac{\|\sigma_h\|_{L^2}}{\|\sigma_h(\cdot,T)\|_{L^2}}$ and $\frac{\|\theta_h\|_{L^2}}{\|\theta_h(\cdot,T)\|_{L^2}}$ ($T=20$) against time in Fig. 5. From Figs. 4 and 5, we can see that the magnetic field $\sigma=\mathrm{curl}\mathbf{A}$ arrives at stationary state earlier than the electric

https://doi.org/10.4208/cicp.OA-2016-0120 Published online by Cambridge University Press

Table 4: The average iterations required by the new approach and the conventional FEM for the vortex motion simulation on the unit square domain (Example 4.1).

	New approach				Conventional FEM	
$\tau=0.01$	Iter(ψ)	Iter(σ)	Iter(θ)	Iter($\mathbf{A}$)	Iter(ψ)	Iter($\mathbf{A}$)
M=32	10.46	12.77	46.87	13.95	10.40	33.64
M=64	13.96	22.88	87.88	12.02	13.94	60.57
M=128	23.36	35.11	169.90	10.34	23.36	115.37
M=256	43.61	45.47	330.88	9.29	43.60	225.38
$\tau=0.005$	Iter(ψ)	Iter(σ)	Iter(θ)	Iter($\mathbf{A}$)	Iter(ψ)	Iter($\mathbf{A}$)
M=32	11.51	7.57	38.21	13.06	11.44	24.13
M=64	10.06	10.28	71.16	11.05	10.04	46.42
M=128	16.38	14.65	134.54	9.58	16.37	90.29
M=256	29.07	20.45	263.57	8.13	29.06	177.35
$\tau=0.001$	Iter(ψ)	Iter(σ)	Iter(θ)	Iter($\mathbf{A}$)	Iter(ψ)	Iter($\mathbf{A}$)
M=32	11.42	2.59	17.75	11.12	11.38	10.51
M=64	9.11	2.96	33.49	9.07	9.12	20.22
M=128	6.76	2.97	64.91	7.34	6.73	38.80
M=256	11.67	3.44	126.11	6.66	11.69	74.39

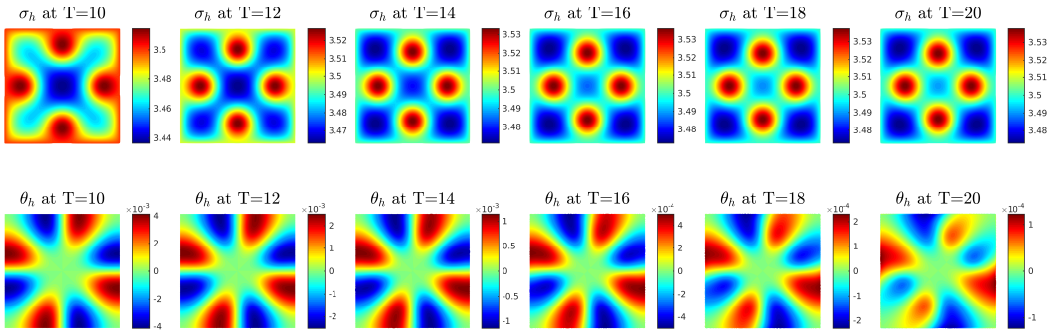


Figure 4: σ_h and θ_h computed by the new approach at $T=10$, 12, 14, 16, 18 and 20. A linear element method with $M=128$ and $\tau=0.01$ are used (Example 4.1).

potential $\theta=\text{div}\mathbf{A}$. For $t>1$, Fig. 5 shows that $\frac{\|\sigma_h\|_{L^2}}{\|\sigma_h(\cdot,20)\|_{L^2}}\approx 1$. Fig. 4 shows clearly that σ_h is almost stable at $T=12$. On the contrary, $\frac{\|\theta_h\|_{L^2}}{\|\theta_h(\cdot,20)\|_{L^2}}$ changes drastically in the whole time interval, see Figs. 4 and 5. The amplitude of θ_h is 4.0×10^{-3} at $T=10$ and shrinks to 1.0×10^{-4} at $T=20$. Clearly, at time t_n, the initial guess θ_h^{n-1} for the CG solver is far from θ_h^n and more iterations are needed.

https://doi.org/10.4208/cicp.OA-2016-0120 Published online by Cambridge University Press

Table 5: The condition numbers of the coefficient matrices by the new approach and the conventional FEM for the vortex motion simulation on the unit square domain (Example 4.1).

	New approach				Conventional FEM	
$\tau=0.01$	Cond(ψ)	Cond(σ)	Cond(θ)	Cond($\mathbf{A}$)	Cond(ψ)	Cond($\mathbf{A}$)
M=32	6.21	2572.81	88.96	14.62	6.21	2918.48
M=64	9.01	10269.53	339.63	14.65	9.01	11390.93
M=128	18.28	41056.43	1332.82	14.66	18.28	45116.78
M=256	56.97	164204.07	5285.43	14.66	56.97	179675.62
$\tau=0.005$	Cond(ψ)	Cond(σ)	Cond(θ)	Cond($\mathbf{A}$)	Cond(ψ)	Cond($\mathbf{A}$)
M=32	7.52	2804.44	45.97	14.62	7.52	3099.02
M=64	7.27	11192.55	170.91	14.65	7.27	11959.44
M=128	12.13	44745.05	667.36	14.66	12.13	47266.55
M=256	30.99	178955.05	2643.60	14.66	30.99	188151.18
$\tau=0.001$	Cond(ψ)	Cond(σ)	Cond(θ)	Cond($\mathbf{A}$)	Cond(ψ)	Cond($\mathbf{A}$)
M=32	12.06	3022.18	13.63	14.62	12.06	3739.05
M=64	8.25	12059.70	37.43	14.65	8.25	12908.63
M=128	6.87	48210.10	135.76	14.66	6.87	49475.15
M=256	10.91	192811.78	530.46	14.66	10.91	195778.79

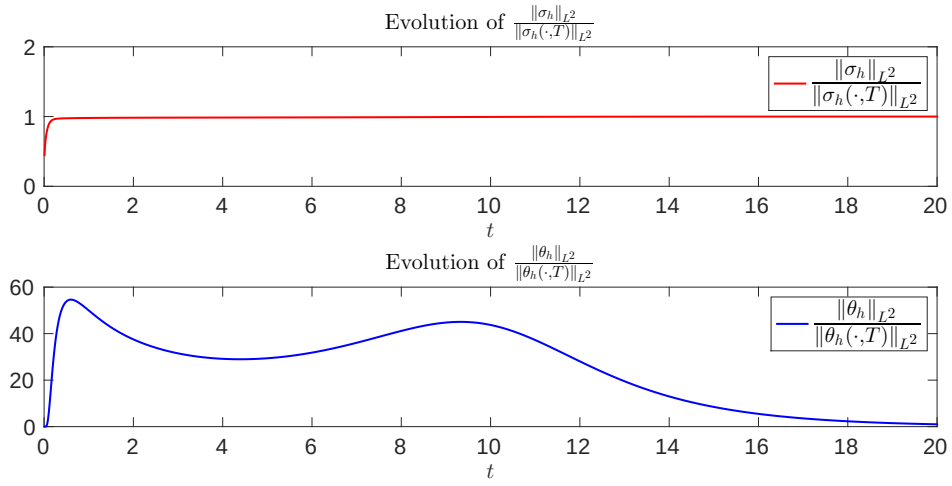


Figure 5: Evolution of $\frac{\|\sigma_h\|_{L^2}}{\|\sigma_h(\cdot,T)\|_{L^2}}$ and $\frac{\|\theta_h\|_{L^2}}{\|\theta_h(\cdot,T)\|_{L^2}}$ computed by the new approach. $T=20$. A linear element method with $M=128$ and $\tau=0.01$ are used. (Example 4.1)

https://doi.org/10.4208/cicp.OA-2016-0120 Published online by Cambridge University Press

Example 4.2. In this example, we use the proposed method to study the vortex motion in an L-shape superconductor (see Fig. 6). Here, the Ginzburg-Landau parameter $\kappa=10$ and the applied magnetic field $H_e=5$. We set the initial conditions to be the perfectly superconducting state with $\psi_0=0.8+i0.6$ and $\mathbf{A}_0=[0,0]^T$. This example was tested by several different methods, e.g., see [15, 16, 21]. The regularity of the GL equations in polygons was studied in [20]. For the L-shape domain in spatial direction, we have

$$\psi\in\mathcal{H}^{1+s}(\Omega),\quad \mathbf{A}\in\mathbf{H}^s(\Omega),\quad \mathrm{div}\mathbf{A},\mathrm{curl}\mathbf{A}\in H^{1+s}(\Omega),\quad \frac{1}{2}<s<\frac{2}{3}. \tag{4.1}$$

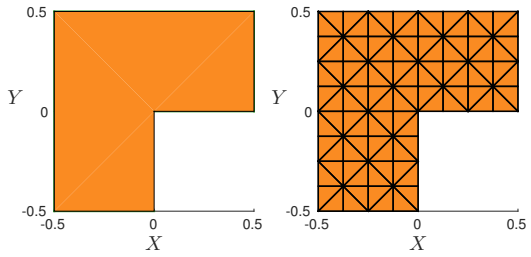


Figure 6: A uniform triangular mesh on the L-shape domain with $M=8$ (Example 4.2).

We solve the GL equations (2.1)-(2.4) by the proposed method on a uniform triangular partition with $M=128$, where $\tau=0.01$ and a linear finite element approximation are used. In Fig. 7, we plot $|\psi_h|$, θ_h and σ_h at $T=1$, 5, 10, 15 and 20. From Fig. 7, we can observe that one vortex enters the material from the re-entrant corner as the time increases. The vortex patterns shown in Fig. 7 are also similar to those reported in [15,21], where a mixed method and a numerical method based on Hodge decomposition were used, respectively. However, the conventional Lagrange FEM for solving the GL equations under Lorentz gauge may converge to an incorrect solution, see [15,21].

We also test the spatial convergence rate of the proposed method (2.21)-(2.24). Here, the terminal time $T=2.0$. We use a very small fixed time step $\tau=1.0\times10^{-4}$. Since the exact solution is unavailable, numerical solution with a linear element method with $M=512$ is used as the exact solution. To test the spatial convergence rate, we use a linear element method on gradually refined meshes with $M=16$, 32, 64, 128. The L^2 errors are given in Table 6. From Table 6, we can see that the convergence rates for ψ, σ, θ and $\mathbf{curl}\sigma$ are around $h^{1.5}$ while the convergence rate for $\mathbf{A}$ is about $h^{0.7}$, which agree with the spatial regularity (4.1). It should be noted that the convergence rate displayed in Table 6 is lower than that of Example 3.1, where the exact solution is smooth.

Example 4.3. Finally, we use the proposed method to study the vortex motion in a circular disk with boundary defect. Here, the Ginzburg-Landau parameter $\kappa=4.0$ and the applied magnetic field $H_e=0.9$. Again, we set the initial conditions to be the perfectly superconducting state with $\psi_0=0.8+i0.6$ and $\mathbf{A}_0=[0,0]^T$. This example was used in [1] to investigate the influence of geometry on vortex motion. This example was also tested by several different methods, e.g., see [15,21].

https://doi.org/10.4208/cicp.OA-2016-0120 Published online by Cambridge University Press

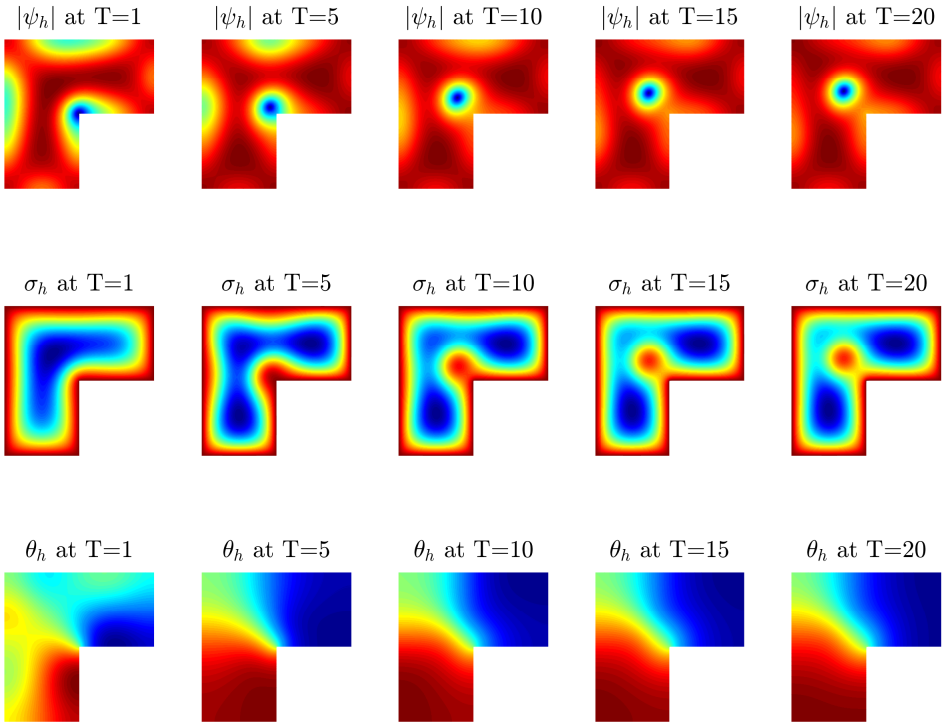


Figure 7: $|\psi_h|$ (upper), σ_h (middle) and θ_h (lower) computed by the new approach at $T=1$, 5, 10, 15 and 20. A linear element method with $M=128$ and $\tau=0.01$ are used (Example 4.2).

Table 6: L^2-norm errors of the new approach with a linear element method on the L-shape domain at $T=2.0$ with $\tau=1.0\times10^{-4}$ (Example 4.2).

	Err_ψ	Err_σ	Err_θ	$\mathrm{Err}_{\mathbf{A}}$	$\mathrm{Err}_{\mathbf{curl}\sigma}$
$M=16$	5.5920e-02	2.7586e-03	3.3285e-03	6.4717e-02	2.1947e-02
$M=32$	2.1019e-02	8.7451e-04	1.2195e-03	3.9689e-02	7.4094e-03
$M=64$	7.7711e-03	2.8373e-04	4.4753e-04	2.4791e-02	2.5471e-03
$M=128$	2.7054e-03	8.9990e-05	1.5579e-04	1.5229e-02	8.7669e-04
order	1.46	1.65	1.47	0.70	1.55

A quadratic element method($r=2$) on a regular mesh with 10428 vertices and 20532 elements and $\tau=0.002$ are used in our computation. In Fig. 8, we plot $|\psi_h|$, θ_h and σ_h at $T=1$, 20, 40, 80, 160 and 200. From Fig. 8, we can observe that vortices enter the material and then arrive at the stationary state as the time increases. For comparison, we refer to [15] and [21], where a mixed method and a numerical method based on Hodge decomposition were used, respectively. However, the results obtained in [1] by the conventional

https://doi.org/10.4208/cicp.OA-2016-0120 Published online by Cambridge University Press

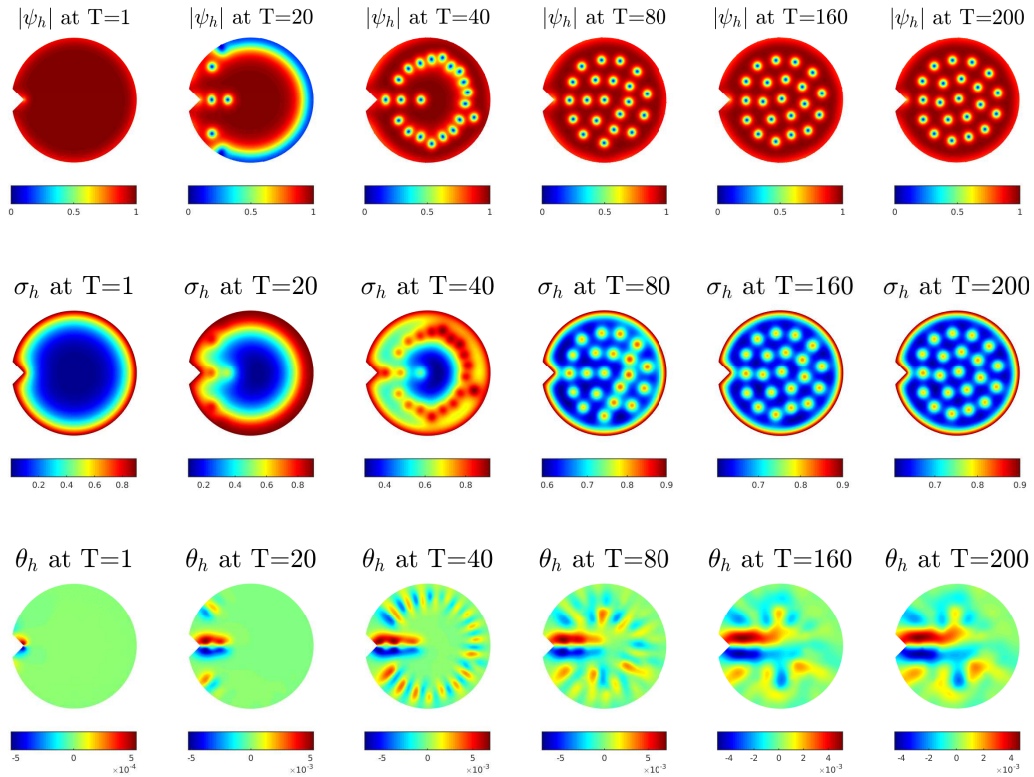


Figure 8: $|\psi_h|$ (upper), σ_h (middle) and θ_h (lower) computed by the new approach at $T=1$, 20, 40, 80, 160 and 200. A quadratic element method with 10428 vertices and 20532 elements and $\tau=0.002$ are used (Example 4.3).

Lagrange FEM showed that there is a giant vortex near the defect. As remarked in [21], numerical results in [1] is probably incorrect.

5 Conclusions

We have proposed a new linearized FEM for the GL equations under the Lorentz gauge. Numerical experiments illustrate that the proposed method is efficient, accurate and robust. In particular, the method provides optimal convergence rates for three physical components: the order parameter ψ, the magnetic field σ and the electric potential θ. Moreover, the new approach is well suitable for vortex simulations in complex geometries including non-convex domains, which are of high interests in many applications. The mixed formulation and numerical methods presented in this paper are based on the GL equations in two-dimensional space. Extension to the three-dimensional model is under going.

https://doi.org/10.4208/cicp.OA-2016-0120 Published online by Cambridge University Press

Acknowledgments

The work of the author was supported in part by a grant from the National Natural Science Foundation of China (NSFC) under grant No. 11501227 and Fundamental Research Funds for the Central Universities, HUST, China, under Grant No. 2014QNRC025, No. 2015QN13. The author would like to thank Dr. Kui Du for useful suggestions.

References

[1] T. Alstrom, M. Sorensen, N. Pedersen and S. Madsen, Magnetic flux lines in complex geometry type-II superconductors studied by the time dependent Ginzburg-Landau equation, *Acta Appl. Math.*, 115(2011), 63–74.
[2] M. Benzi, G. Golub and J. Liesen, Numerical solution of saddle point problems, *Acta Numerica*, 14(2005), 1–137.
[3] F. Bethuel, H. Brezis and F. Hélein, *Ginzburg-Landau Vortices*, Progress in Nonlinear Partial Differential Equations and Their Applications 13, Birkhäuser Boston, Boston, 1994.
[4] S. Brenner and L. Scott, *The Mathematical Theory of Finite Element Methods*, Springer, New York, 2002.
[5] L. Chen, Y. Wu, L. Zhong and J. Zhou, Multigrid preconditioners for mixed finite element methods of vector Laplacian, *arXiv:1601.04095.*
[6] Z. Chen, Mixed finite element methods for a dynamical Ginzburg-Landau model in superconductivity, *Numer. Math.*, 76(1997), 323–353.
[7] Z. Chen and K. Hoffmann, Numerical studies of a non-stationary Ginzburg-Landau model for superconductivity, *Adv. Math. Sci. Appl.*, 5(1995), 363–389.
[8] Z. Chen, K. Hoffmann and J. Liang, On a non-stationary Ginzburg-Landau superconductivity model, *Math. Methods Appl. Sci.*, 16(1993), 855–875.
[9] K. Chrysafinos and L. Hou, Error estimates for semidiscrete finite element approximations of linear and semilinear parabolic equations under minimal regularity assumptions, *SIAM J. Numer. Anal.*, 40(2002), 282–306.
[10] Q. Du, Finite element methods for the time-dependent Ginzburg-Landau model of superconductivity, *Comput. Math. Appl.*, 27(1994), 119–133.
[11] Q. Du, M. Gunzburger and J. Peterson, Analysis and approximation of the Ginzburg-Landau model of superconductivity, *SIAM Rev.*, 34(1992), 54–81.
[12] J. Fleckinger-Pelle and H. Kaper, Gauges for the Ginzburg-Landau equations of superconductivity, *Z. Angew. Math. Mech.*, 76(S2)(1996), 345–348.
[13] H. Frahm, S. Ullah and A. Dorsey, Flux dynamics and the growth of the superconducting phase, *Phys. Rev. Lett.*, 66(1991), 3067–3070.
[14] H. Gao, B. Li and W. Sun, Optimal error estimates of linearized Crank-Nicolson Galerkin FEMs for the time-dependent Ginzburg-Landau equations in superconductivity, *SIAM J. Numer. Anal.*, 52(2014), 1183–1202.
[15] H. Gao and W. Sun, An efficient fully linearized semi-implicit Galerkin-mixed FEM for the dynamical Ginzburg-Landau equations of superconductivity, *J. Comput. Phys.*, 294(2015), 329–345.
[16] H. Gao and W. Sun, A new mixed formulation and efficient numerical solution of Ginzburg-Landau equations under the temporal gauge. *SIAM J. Sci. Comput.*, 38(2016), A1339–A1357.

https://doi.org/10.4208/cicp.OA-2016-0120 Published online by Cambridge University Press

[17] W. Gropp, H. Kaper, G. Leaf, D. Levine, M. Palumbo and V. Vinokur, Numerical simulation of vortex dynamics in type-II superconductors, *J. Comput. Phys.*, 123(1996), 254–266.
[18] D. Gunter, H. Kaper and G. Leaf, Implicit integration of the time-dependent Ginzburg-Landau equations of superconductivity, *SIAM J. Sci. Comput.*, 23(2002), 1943–1958.
[19] S. Kim, J. Burkardt, M. Gunzburger, J. Peterson and C. Hu, Effects of sample geometry on the dynamics and configurations of vortices in mesoscopic superconductors, *Phys. Rev. B*, 76(2007), 024509.
[20] B. Li and Z. Zhang, Mathematical and numerical analysis of time-dependent Ginzburg-Landau equations in nonconvex polygons based on Hodge decomposition, *Math. Comp.*, 86(2017), 1579–1608.
[21] B. Li and Z. Zhang, A new approach for numerical simulation of the time-dependent Ginzburg-Landau equations, *J. Comput. Phys.*, 303(2015), 238–250.
[22] A. Logg, K. Mardal and G. Wells (Eds.), *Automated Solution of Differential Equations by the Finite Element Method*, Springer, Berlin, 2012.
[23] M. Mu, A linearized Crank-Nicolson-Galerkin method for the Ginzburg-Landau model, *SIAM J. Sci. Comput.*, 18(1997), 1028–1039.
[24] M. Mu and Y. Huang, An alternating Crank-Nicolson method for decoupling the Ginzburg-Landau equations, *SIAM J. Numer. Anal.*, 35(1998), 1740–1761.
[25] L. Peng, Z. Wei and D. Xu, Vortex states in mesoscopic superconductors with a complex geometry: A finite element analysis, *Int. J. Mod. Phys. B*, 28(2014), 1450127,
[26] N. Raza, S. Sial and S. Siddiqi, Approximating time evolution related to Ginzburg-Landau functionals via Sobolev gradient methods in a finite-element setting, *J. Comput. Phys.*, 229(2010), 1621–1625.
[27] W. Richardson, A. Pardhanani, G. Carey and A. Ardelea, Numerical effects in the simulation of Ginzburg-Landau models for superconductivity, *Int. J. Numer. Meth. Engng.*, 59(2004), 1251–1272.
[28] C. Yang, A linearized Crank-Nicolson-Galerkin FEM for the time-dependent Ginzburg-Landau equations under the temporal gauge, *Numer. Methods Partial Differential Equations*, 30(2014), 1279–1290.
[29] Y. Zhang, Z. Sun and T. Wang, Convergence analysis of a linearized Crank-Nicolson scheme for the two-dimensional complex Ginzburg-Landau equation, *Numer. Methods Partial Differential Equations*, 29(2013), 1487–1503.

https://doi.org/10.4208/cicp.OA-2016-0120 Published online by Cambridge University Press